Energy & Environmental Science

PAPER

View Article Online
View Journal | View Issue

Cite this: *Energy Environ. Sci.*, 2017, **10**, 1003

High power densities created from salinity differences by combining electrode and Donnan potentials in a concentration flow cell†

Taeyoung Kim, Bruce E. Logan and Christopher A. Gorski *

Received 18th January 2017,
Accepted 20th March 2017

DOI: 10.1039/c7ee00188f

rsc.li/ees

Recent estimates suggest that approximately 40% of global electricity demands can be met by capturing the potential energy contained in the mixing of seawater and freshwater at coasts. Several technologies are currently being explored to capture this energy and maximize the achievable electrical power density. Here we report a new method to capture this energy that yielded a peak power density of 12.6 ± 0.5 W m^{-2}-membrane area (average = 3.8 ± 0.1 W m^{-2}), which is the highest value reported to date for salinity gradient energy technologies fed with synthetic seawater (30 g L^{-1} NaCl) and freshwater (1 g L^{-1} NaCl). This unprecedentedly high power density was achieved in a concentration flow cell containing non-toxic copper hexacyanoferrate electrodes that developed electrode potentials based on Na^+ activities and an anion-exchange membrane that developed a Donnan potential based on Cl^- activities. The peak power density increased to 26.3 ± 1.3 W m^{-2} (average = 9.4 ± 0.9 W m^{-2}) when using a highly saline synthetic brine (300 g L^{-1} NaCl) and freshwater (1 g L^{-1} NaCl). Stacking two flow cells in series doubled the total power while maintaining the same power per membrane area. Combining electrode and Donnan potentials in a concentration flow cell offers a new means to harvest salinity gradient energy that may lead to an economically viable technology.

Broader context

Combining two waters with different salt concentrations (*e.g.*, seawater and freshwater) produces mixing energy, which can theoretically generate an enormous amount of carbon-neutral renewable electricity. Several salinity gradient energy (SGE) technologies are being explored to convert salinity differences into electrical power, based on osmotic pressure differences, such as pressure-retarded osmosis (PRO), or electrochemical processes, such as reverse electrodialysis (RED) and capacitive mixing (CapMix). There are currently challenges with all these approaches. PRO is susceptible to membrane fouling, and CapMix and RED yield low power densities. Here, we tested a new technology – a concentration flow cell – that combined the mechanisms responsible for power production in CapMix and RED to generate an unprecedentedly high power density for an electrochemical system. This system is a critical step towards making SGE technologies both efficient and affordable.

Introduction

The difference in salt concentrations between freshwater and seawater contains a tremendous amount of potential energy. Globally, the flow of rivers into oceans and seas at coasts is estimated to contain 1.9 TW of power.[1,2] Approximately 1 TW of this power is realistically harvestable when accounting for geography and other practical constraints,[3] which amounts to 40% of the worldwide electricity generated in 2012 (21 600 TW h).[4] Waters that have higher salt concentrations than seawater (*e.g.*, hypersaline lakes, geothermal wells, reject flows from desalination plants, and hydraulic fracturing flowback water) contain even larger energy densities when combined with freshwater on a volumetric basis,[5,6] but they have been less extensively studied because the total available volumes are small relative to seawater and technical challenges in harvesting the potential energy.[7–9]

Multiple approaches are currently being explored to convert salinity differences into electricity by either creating hydraulic pressure or utilizing electrochemical principles. The technique that has received the most attention to date, pressure retarded osmosis (PRO), uses semi-permeable membranes that selectively allow water transport through the membrane – while rejecting salt – to convert osmotic pressure into hydraulic head.[3,6,10,11] PRO has produced the highest power densities to date for synthetic seawater and freshwater (calculated: 9.2 W m^{-2}-membrane area, measured: 7.5 W m^{-2}),[11,12] but its feasibility is marred by rapid

Department of Civil and Environmental Engineering, The Pennsylvania State University, University Park, PA 16802, USA. E-mail: gorski@engr.psu.edu; Fax: +1-814-863-7304; Tel: +1-814-865-5673

† Electronic supplementary information (ESI) available. See DOI: 10.1039/c7ee00188f

membrane fouling, which decreases electricity production and increases maintenance costs.[13–15] PRO is also poorly suited for harvesting energy from hypersaline waters, as the semi-permeable membranes currently used cannot withstand the necessary pressures.[16]

Techniques that rely on electrochemical principles have been studied less extensively than PRO, but have recently been gaining attention due in part to increasing performance.[17–24] These techniques develop cell voltages by creating electrochemical potentials using salinity differences between two waters. The potentials can be created across ion-exchange membranes as a result of selective ion transport (*i.e.*, Donnan potentials) or at electrode–water interfaces due to interactions between electrodes and ionic species (*i.e.*, electrode potentials). Generally, technologies that develop cell voltages primarily through Donnan potentials are referred to as reverse electrodialysis (RED) systems,[3,10,24–27] while technologies that develop cell voltages primarily through capacitive or pseudo-capacitive electrode-based reactions are referred to as capacitive mixing (CapMix) systems.[17–23] RED and CapMix have not been considered commercially viable yet because the maximum reported power densities (2.9 W m^{-2} in RED,[26] 0.4 W m^{-2} in CapMix[28]) are lower than estimated values of what would be needed to make them economically competitive with conventional renewable technologies.[29] There have been multiple efforts at scaling up RED systems in pilot plants, which have yielded 0.8 W m^{-2} using real brackish water and brine, but these systems have not been commercialized.[30,31] One potential reason for the relatively low power densities in RED and CapMix systems compared to PRO is that these electrochemical systems have been designed to primarily exploit only one type of potential, with little work attempting to take advantage of electrode and Donnan potentials when both are present within the same cell.[18,21,22,32–34]

Here, we report that combining electrode and Donnan potentials in an electrochemical cell fed with synthetic freshwater and seawater led to peak power densities that were unprecedentedly high compared to previously reported electrochemical systems, and on par with the maximum calculated values for PRO. To study this process, we constructed a concentration flow cell in which two identical electrodes composed of copper hexacyanoferrate (CuHCF) were separated by an anion-exchange membrane. One channel of the cell was fed with synthetic seawater, while the other channel was fed with synthetic freshwater. Periodically switching the solution flow paths allowed the cell to recharge and further produce power. We examined how the cutoff voltage used for switching flow paths, external resistance, and salt concentrations influenced peak and average power production. Based on these results, we identified how stacking multiple cells influenced electricity production and evaluated the energy efficiency.

Materials and methods

Electrode preparation

Copper hexacyanoferrate (CuHCF) was synthesized using a co-precipitation method.[35] Briefly, 0.1 M $Cu(NO_3)_2$ (80 mL, Sigma Aldrich) and 0.05 M $K_3[Fe(CN)_6]$ (80 mL, J.T. Baker) solutions were simultaneously added drop-wise to deionized water (40 mL) under vigorous stirring at room temperature, which immediately formed precipitates. These precipitates were collected by centrifugation and then dried overnight at 70 °C. Material characterizations (X-ray diffraction and scanning electron microscope) are provided in ESI† (Fig. S1 and S2). The electrode slurry consisting of CuHCF (70 wt%), carbon black (20 wt%, Vulcan XC72R, Cabot) and polyvinyledenefluoride (10 wt%, kynar HSV 900, Arkema Inc.) was prepared in 1-methyl-2-pyrrolidinone (2 mL per 0.1 g CuHCF, Sigma Aldrich). This slurry was loaded drop-wise onto carbon cloth (1071HCB, AvCarb Material Solutions) followed by overnight drying in a vacuum oven at 70 °C. The mass loading of the electrode material was approximately 4.7 mg cm^{-2}.

Cell construction

All experiments were performed in a custom-built flow cell (Fig. S3, ESI†). This cell consisted of two channels (width = 1 cm; height = 3 cm; thickness = ~120 μm) that were separated by an anion-exchange (Selemion AMV, Asahi Glass, Japan), cation-exchange membrane (Selemion CMV), or non-selective membrane (Celgard® 3501). The CuHCF electrodes were placed in each channel, and graphite foil was used as a current collector. The cell was sealed using two end plates with bolts and nuts.

Energy harvesting experiments

Low concentration (LC; 1 g L^{-1}, representative of freshwater) and high concentration (HC; 30 g L^{-1}, representative of seawater) NaCl solutions prepared by dissolving NaCl (Macron Fine Chemicals™) in deionized water (Synergy®, EMD Millipore) were used to evaluate the energy harvesting performance of the system, unless otherwise stated. These solutions were fed to each channel of the cell using a peristaltic pump (Cole-Parmer) at a flow rate of 15 mL min^{-1}. Power production was achieved by connecting two electrodes with external resistors (R_{ext} = 2, 3, 4, 6, 10 Ω), and the cell voltage (ΔE) was recorded using a potentiostat (VMP3, Bio-Logic). Power produced from the cell was calculated from the recorded cell voltage and the R_{ext} ($P = \Delta E^2/R_{ext}$), and the power density was obtained by dividing the produced power by the membrane area (~3 cm^2). The average power density was calculated from the power densities of a cycle, and multiplying it with cycle time produced the energy density. Each cycle started by switching the flow path of HC and LC solutions, and ended when the cell voltage decreased below cutoff voltages (5, 10, 30, 50, 70 mV). Note that we did not use constant current discharge tests to determine the average power density because this method only accounted for the discharge process, while the method used here (*i.e.*, connecting the external resistance during the entire process) accounted for both charge and discharge processes, which should be included when calculating energy and average power densities in our system. Different combinations of LC (0.6, 1.0, 2.5 g L^{-1}) and HC (30, 60, 300 g L^{-1}) NaCl solutions were used to test power and energy recoveries from brines and brackish waters. Cell stacking was demonstrated by assembling two cells in series (Fig. S4, ESI†). For testing this double-stacked

cell, a flow rate was adjusted from 15 to 30 mL min^{-1}, which produced the same hydraulic retention time as a single cell.

Measurement of open-circuit cell voltage

To determine the gained voltage of the concentration flow cell depending on the type of membrane used and salinity difference, we recorded open-circuit cell voltages while feeding two solutions at 15 mL min^{-1}. The effect of membrane on the open-circuit cell voltage was examined using anion-exchange, cation-exchange, or non-selective membranes without CuHCF (only with carbon cloth). The contribution of CuHCF electrodes was examined using a non-selective membrane. Lastly, the open-circuit cell voltage was recorded by combining the CuHCF electrodes with anion-exchange, cation-exchange, or non-selective membranes. The effect of salinity differences was evaluated in a cell consisting of the anion-exchange membrane and the CuHCF electrodes by using a fixed LC solution (1 g L^{-1}) while changing the concentration of HC solution (2.5, 4, 6, 10, 15, 30, 60, 100, 300 g L^{-1}). Visual MINTEQ (version 3.0) was used to calculate activity-corrected cell voltages (SIT method) from the salinity differences.

Evaluating energy efficiency

The energy efficiency was calculated by dividing the net energy harvested in the concentration flow cell by the theoretical available energy from a salinity difference (HC = 30 g L^{-1}; LC = 1 g L^{-1}). The net harvested energy of the cell was evaluated based on several experiments and assumptions, in which two main processes were taken into account: (1) release/uptake of ions by electrodes due to redox reactions and transport of ions through the anion-exchange membrane, and (2) dilution/concentration caused by exchanging solutions between channels (Supplementary Note 1, ESI†).

Results & discussion

Power production performance from synthetic seawater and freshwater

Electrical power was produced in the concentration flow cell by connecting two identical CuHCF electrodes with an external resistor (R_{ext} = 6 Ω) while flowing HC (30 g L^{-1}) and LC (1 g L^{-1}) NaCl solutions through two channels separated by an anion-exchange membrane (Fig. 1a). Over the course of a cycle, the cell voltage and power initially increased for approximately five seconds, then gradually decreased as redox reactions occurred at the CuHCF electrodes (Fig. 1b), as explained below. After completing the first discharge cycle, switching the flow path between HC and LC solutions reversed the cell voltage, leading to further power production in subsequent cycles. We determined the peak power density that could be produced in the concentration flow cell by measuring power density (*i.e.*, power divided by membrane area) as a function of cutoff cell voltage (*i.e.*, the cell voltage value used to trigger switching the HC and LC solution flow paths, Fig. 2a). When the cutoff voltage was 5 mV (R_{ext} = 6 Ω), the peak power density was 12.6 ± 0.5 W m^{-2} (± std. dev.). Increasing the cutoff voltage decreased the peak power density, since a larger cutoff voltage meant that the cell was discharged to a lesser extent before recharging, leading to a smaller cell voltage when the solutions were switched. The peak power density achieved here was the highest value reported for synthetic seawater and freshwater when compared to PRO (calculated: 9.2 W m^{-2}, measured: 7.5 W m^{-2}),[11,12] RED (2.9 W m^{-2}),[26] and CapMix (0.4 W m^{-2}).[28]

For the concentration flow cell, there was a tradeoff between the peak power production over a portion of a cycle and the maximum average power density that could be achieved over a complete cycle (Fig. 2b). Unlike the peak power density, which was larger at lower cutoff voltages, the average power density

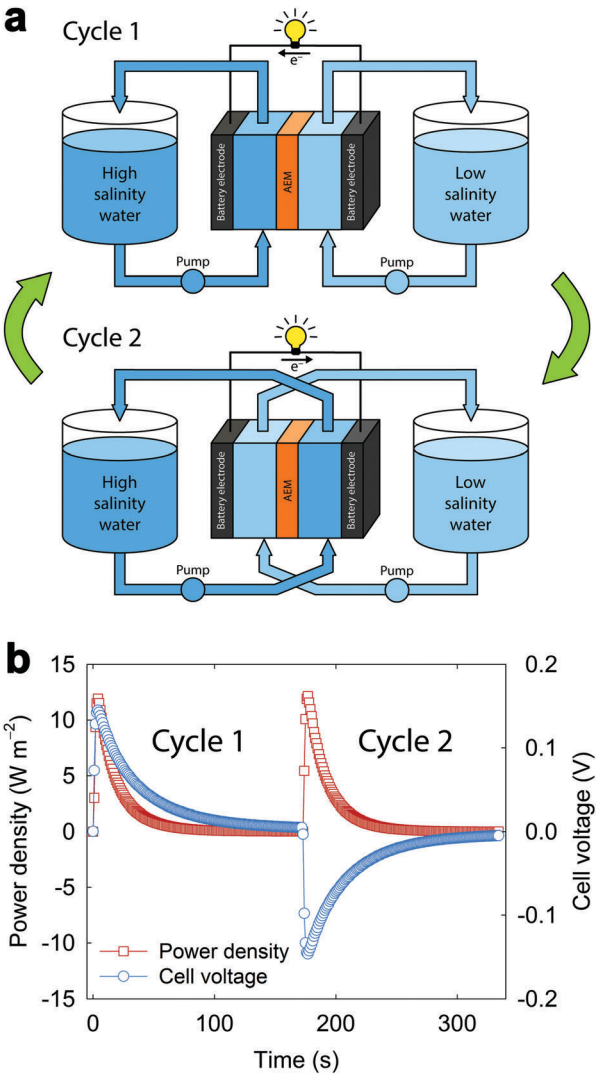

Fig. 1 (a) Schematic diagram of the concentration flow cell for harvesting energy from salinity differences. The power production was achieved by using two identical battery electrodes in the cell while feeding high salinity water and low salinity water through two channels separated by an anion-exchange membrane (AEM). After completing the first cycle, the flow path was switched between high salinity water and low salinity water, leading to power production in the sequel cycle. (b) Representative power density and cell voltage profiles using 1 and 30 g L^{-1} NaCl solutions (R_{ext} = 6 Ω).

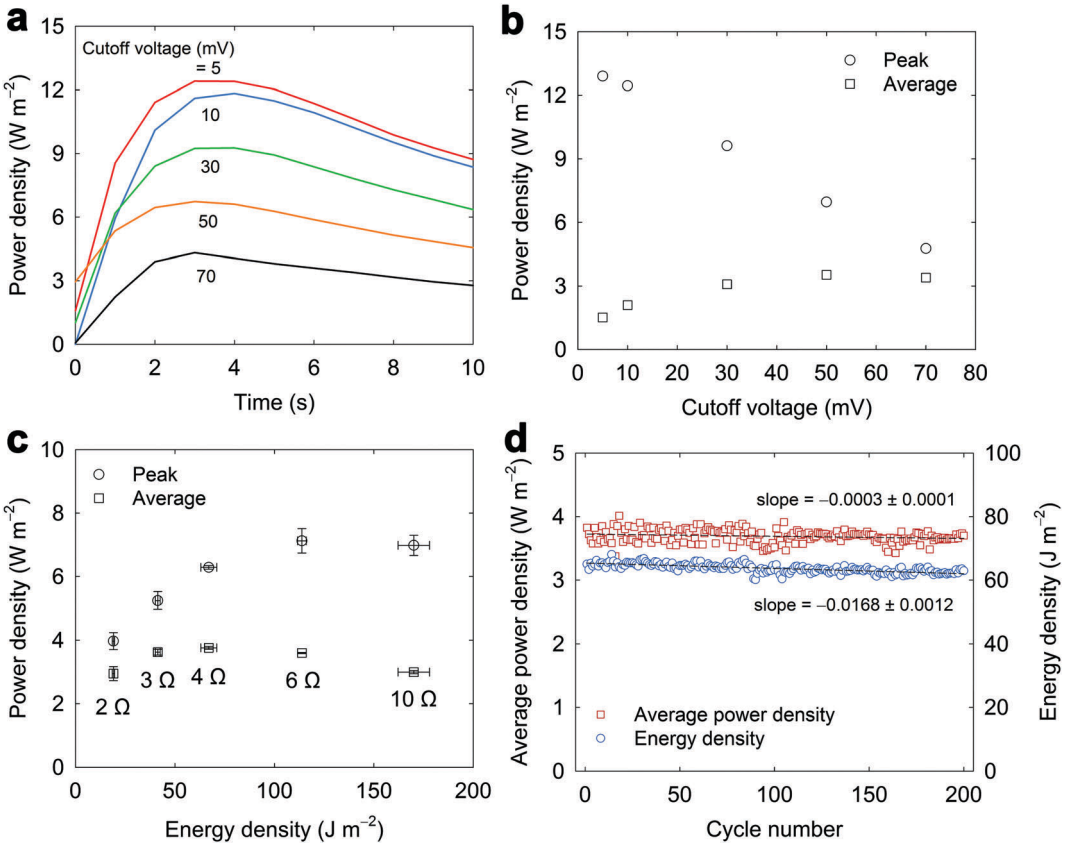

Fig. 2 Energy harvesting performance of the concentration flow cell. (a) Representative power density profiles collected by varying cutoff voltage (R_{ext} = 6 Ω). (b) The effect of cutoff voltage on peak and average power densities (R_{ext} = 6 Ω). (c) Peak and average power densities *vs.* energy density plot as a function of R_{ext} (cutoff voltage = 50 mV). (d) Average power densities and energy densities recorded for 200 cycles (R_{ext} = 4 Ω, cutoff voltage = 50 mV).

was larger at higher cutoff voltages. The maximum average power density for a complete cycle was achieved when the cutoff voltage was 50 mV (3.5 W m^{-2}, R_{ext} = 6 Ω). At the 50 mV cutoff voltage, we measured power production as a function of the external resistance (R_{ext}) applied to the circuit (Fig. 2c and Fig. S9, ESI†). At R_{ext} = 4 Ω, the maximum average power density was 3.8 ± 0.1 W m^{-2}, the peak power density was 6.3 ± 0.1 W m^{-2}, and the energy density was 67.0 ± 4.0 J m^{-2}. In designing the concentration flow cell, we also observed that several other parameters influenced the average and peak power densities, including the hydraulic retention time inside the cell and the method used to fabricate the electrodes (see Fig. S10–S12, ESI†).

We further examined the performance over 200 cycles to determine if the power production could be sustained (Fig. 2d). The average power density for the first 10 cycles was 3.7 ± 0.1 W m^{-2}, and that for the last 10 cycles was 3.7 ± 0.1 W m^{-2}, indicating that there was no loss in power production after 200 cycles. Unlike the stable average power densities produced over this period, the energy density decreased slightly from 65.0 ± 0.8 J m^{-2} (cycles 1–10) to 62.6 ± 0.6 J m^{-2} (cycles 190–200). Fitting the slope of energy density for the 200 cycles yielded a 5.1% decrease. The decrease in energy density was most likely due to partial dissolution of the CuHCF electrodes. Prior work found that other Prussian blue analogues were most stable under mildly acidic pH conditions and could dissolve at basic pHs.[36,37] This loss could be addressed by adjusting the pH of the influent water or periodically replacing electrodes.

Mechanisms by which cell voltages were created in the concentration flow cell

In the concentration flow cell, the high power density was due to the combination of the electrode potentials developed at the CuHCF electrodes and Donnan potential developed across the anion-exchange membrane (Fig. 3a). The open-circuit voltage created in this cell was 0.315 V when using 1 and 30 g L^{-1} NaCl solutions (Fig. 3b). To understand the relative contributions of potentials from the CuHCF electrodes and the anion-exchange membrane to the overall cell voltage, the open-circuit cell voltage was measured in the presence or absence of identical CuHCF electrodes when the channels were separated by a non-selective membrane (*i.e.*, separator), anion-exchange membrane, or cation-exchange membrane. When the cell contained two CuHCF electrodes and a non-selective membrane, the open-circuit cell voltage was 0.185 V, consistent with our previous results using a similar setup.[28] The open-circuit cell voltage developed as a result of the CuHCF electrodes undergoing a surface and/or intercalation redox reaction with Na^+ ions according to the following half reaction:[38]

$$NaCu[Fe^{III}(CN)_6]_{(s)} + xNa^+_{(aq)} + xe^- = Na_{1+x}Cu[Fe^{II}(CN)_6]_x[Fe^{III}(CN)_6]_{1-x(s)} \quad (1)$$

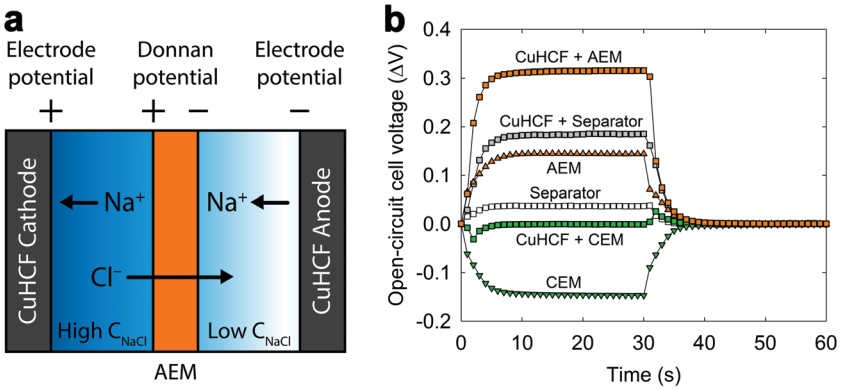

Fig. 3 Developing the cell voltage from salinity differences. (a) Schematic of the cell describing the potential development that was created by CuHCF electrodes (electrode potential) and anion-exchange membrane (AEM) (Donnan potential). (b) The open-circuit cell voltage profiles recorded over time with the flow path switch interval of 30 s. The profiles were obtained using copper hexacyanoferrate (CuHCF) with AEM; CuHCF with a separator; AEM only; a separator only; CuHCF with cation-exchange membrane (CEM); CEM only.

Note that CuHCF is just one of several different Prussian blue analogues or metal hexacyanometalates that can be employed for redox reactions with cations, as several different metals can be incorporated into this general structure.[35,39–43] In the solutions, Na^+ ions were the only active species that could interact with the CuHCF, and therefore the cell voltage (ΔE, V) of the concentration flow cell could be described by combining the Nernst equations of the two electrodes:

$$\Delta E = 2\frac{RT}{F}\ln\left(\frac{a_{Na^+,HC}}{a_{Na^+,LC}}\right) \quad (2)$$

where R is the gas constant (8.314 J mol^{-1} K^{-1}), T is absolute temperature (298 K in our experiments), F is the Faraday constant (96 485 C mol^{-1}), and a is activity. The measured cell voltage (0.185 V) was slightly higher than the calculated value based on activities (0.162 V), which was due to a potential that developed across the non-selective membrane,[28,44] as explained below.

Varying the type of membrane that separated the two channels when only carbon cloth electrodes were present (*i.e.*, the electrodes did not contain CuHCF) led to significant differences in the open-circuit cell voltages that developed. The non-selective membrane developed an open-circuit cell voltage of 0.037 V, indicating that a small junction and/or Donnan potential was created across the membrane (Fig. 3b), consistent with our observations for the flow cell containing CuHCF electrodes discussed above. This potential was most likely a consequence of Cl^- having a higher diffusion coefficient than Na^+ and the non-selective membrane having a minor selectivity for Cl^- (Supplementary Note 2, ESI†). When the flow cell contained an anion-exchange membrane, a positive open-circuit cell voltage (0.145 V) developed in the HC solution side due to the selective Cl^--ion transport from HC to LC solutions (Fig. 3b). The open-circuit cell voltage in this case can be described by the following Nernst equation:

$$\Delta E = 2\frac{RT}{F}\ln\left(\frac{a_{Cl^-,HC}}{a_{Cl^-,LC}}\right) \quad (3)$$

which yielded a calculated open-circuit cell voltage of 0.162 V. One possible reason why there were slight differences between the calculated and measured open-circuit cell voltages for this membrane was that the membrane may not have been perfectly selective (*i.e.*, cation crossover may have occurred), which would have decreased the Donnan potential. When the flow cell contained a cation-exchange membrane, a negative open-circuit cell voltage developed (−0.147 V) due to the selective Na^+-ion transport from HC to LC solutions (Fig. 3b) could be described by the Nernst equation,

$$\Delta E = 2\frac{RT}{F}\ln\left(\frac{a_{Na^+,LC}}{a_{Na^+,HC}}\right) \quad (4)$$

which produced a calculated open-circuit cell voltage of −0.162 V. The difference between the measured and calculated values was likely also due to imperfect selectivity of the cation exchange membrane. Collectively, these results suggest that half of the cell voltage was due to the Donnan potential that developed across the anion-exchange membrane, and the other half of the cell voltage was due to the electrode potentials that developed at the CuHCF electrodes. We confirmed this by combining a cation-exchange membrane with CuHCF electrodes, which produced an open-circuit cell voltage of 0.000 V (Fig. 3b). In this design, the negative cell voltage of the cation-exchange membrane and the positive cell voltage of CuHCF electrodes cancelled each other out.

To the best of our knowledge, there have been no previous reports of producing power using both Donnan and electrode potentials from a salinity gradient in an electrochemical cell, although many studies have evaluated materials that could be used for this purpose. For example, a RED system was recently proposed that contain both ion-exchange membranes and carbon-based electrodes capable of developing electrode potentials.[32] Similarly, previous CapMix studies have used flow carbon electrodes (*i.e.*, suspended carbon particles in a solution) that were separated from the saline and fresh water by an ion-exchange membrane,[34] or covered carbon-based electrodes with ion-exchange membranes or polymers, such that no solution flows between the electrode

and the membrane.[18,21,22,33] In these systems, electrode potentials did not develop because the solution composition adjacent to the electrodes either remained static (in the first two examples) or the electrode was not in direct contact with the solution (in the last example). The concentration flow cell described in the present study differed in that it was able to simultaneously develop electrode and Donnan potentials because the seawater and freshwater directly contacted the electrodes.

Power production performance from highly saline waters

To determine if this concentration flow cell could be used to harvest energy from highly saline source waters (*i.e.*, "brines"), we measured the cell voltage and power density as a function of salt concentration. When we maintained a constant LC concentration (1 g L^{-1}) and varied the HC concentration from 2.5 to 300 g L^{-1}, the open-circuit cell voltage increased from 0.087 to 0.509 V (Fig. 4a), in good agreement with the calculated open-circuit cell voltages from eqn (2) and (3) (Fig. 4b). At high HC concentrations (>30 g L^{-1}), the calculated cell voltage was slightly higher than the measured cell voltage – even after accounting for activity coefficients – likely due to a decrease in the Donnan potential as a consequence of a loss of selectivity in the anion-exchange membrane.[9]

To determine how the power density changed when using highly saline and/or very dilute waters, we measured the achievable average power densities and energy densities by varying the LC and HC concentrations over a range of 0.6 to 300 g L^{-1}. The average power density increased concurrently with the HC solution concentration, when the LC solution concentration was fixed at 1 g L^{-1} (Fig. 4c). Using an HC concentration of 300 g L^{-1} NaCl produced the highest peak power density (26.3 ± 1.3 W m^{-2}, R_{ext} = 6 Ω, cutoff voltage = 5 mV, Fig. S14, ESI†) and highest average power density (9.4 ± 0.9 W m^{-2}, R_{ext} = 3 Ω, cutoff voltage = 50 mV). This average power density was significantly higher than the values achieved using 60 g L^{-1} (5.2 W m^{-2}) and 30 g L^{-1} (3.8 W m^{-2}). The average power density and open-circuit cell voltage values also depended on the LC concentration (Fig. 4d and Fig. S15, ESI†), with higher values observed at lower LC concentrations (and constant HC values). In addition, a higher salinity difference allowed for utilizing an increased portion of the CuHCF electrode capacity for a complete cycle due to the larger potentials that developed. Combining seawater

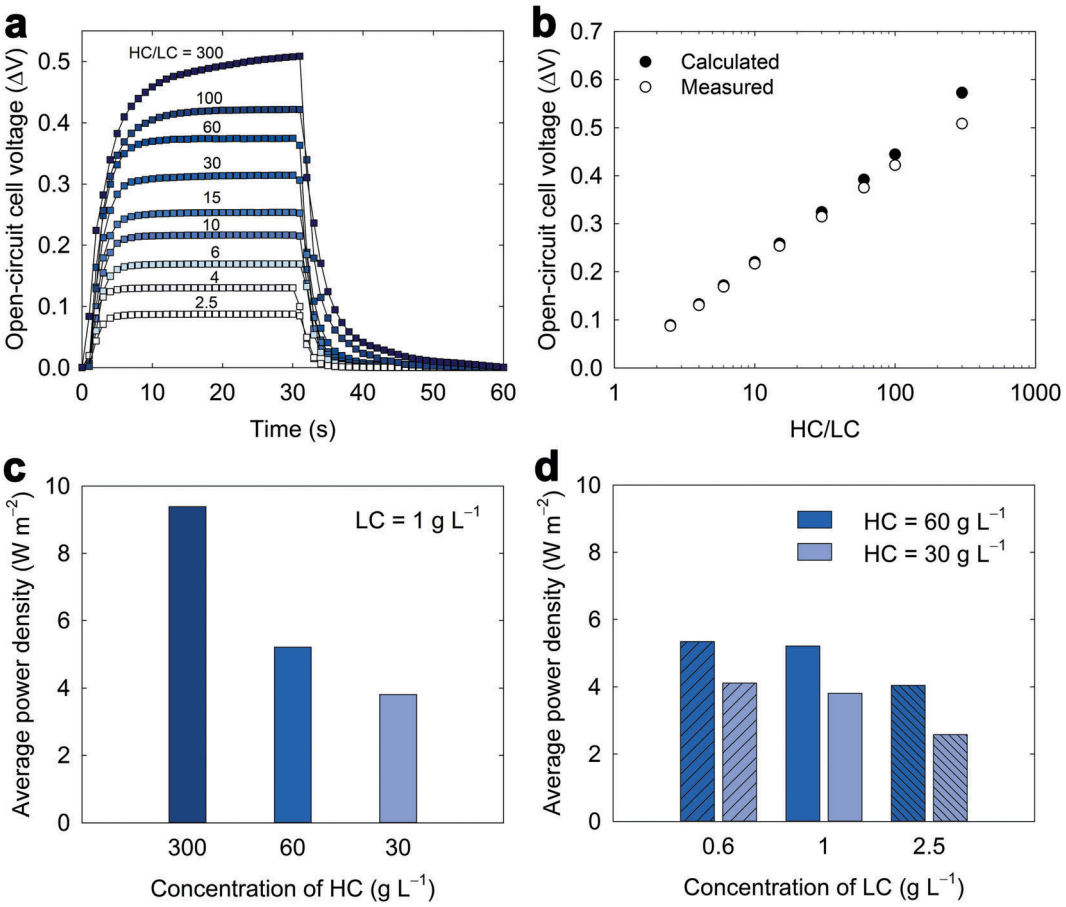

Fig. 4 Demonstration of energy harvesting performance using solutions with different salinities. (a) Open-circuit cell voltage profiles recorded using a low concentration solution (LC, 1 g L^{-1}) and various high concentration solutions (HC, 2.5–300 g L^{-1}). (b) Measured (open circles) and calculated (filled circles) open-circuit cell voltage values as a function of HC/LC ratio (LC = 1 g L^{-1}). (c) The effect of the concentration of HC solutions (30, 60, 300 g L^{-1}) on the average power density (LC = 1 g L^{-1}). The highest average power densities were achieved at R_{ext} = 3 Ω for 300 g L^{-1} and R_{ext} = 4 Ω for 30 and 60 g L^{-1}. (d) The effect of the concentration of LC solutions (0.6, 1, 2.5 g L^{-1}) on the average power density (HC = 30, 60 g L^{-1}, R_{ext} = 4 Ω).

(30 g L^{-1}) with river water (1 g L^{-1}) yielded 338 mC cm^{-2} (R_{ext} = 6 Ω, cutoff voltage = 5 mV), while combining concentrated brine (300 g L^{-1}) with river water (1 g L^{-1}) yielded 554 mC cm^{-2} (R_{ext} = 6 Ω, cutoff voltage = 5 mV) compared to the full capacity of 669 mC cm^{-2} (Fig. S16, ESI†). Combining brackish water with brines or seawater with highly concentrated brines could also be used to produce more energy than using freshwater and seawater, but doing would likely produce a lower power density for the concentration flow cell since power production was primarily controlled by the cell voltages that developed as a result of the salinity difference (Fig. 4c and d). The concentration-dependent cell voltages and power densities indicated that this concentration flow cell could be a viable means to capturing energy from brines, such as water from hypersaline lakes and reject flows from desalination plants, which has been a significant challenge previously reported for CapMix, RED, and PRO systems.[16]

Boosting power production by stacking concentration flow cells

To demonstrate that the overall energy and power production could be increased using multiple concentration flow cells, we measured the energy harvesting performance by stacking two cells in series (*i.e.*, a double-stacked cell) with HC (30 g L^{-1}) and LC (1 g L^{-1}) solutions for synthetic seawater and freshwater. The average power (2.2 mW, R_{ext} = 6 Ω) produced in the double-stacked cell were twice as high as those achieved for a single cell (1.1 mW, R_{ext} = 4 Ω) (Fig. 5). The increased R_{ext} that produced the highest power in the double-stacked cell compared to the single cell was due to the increase in the overall cell resistance caused by stacking two cells in series ($P_{max} = \Delta E^2/4R_{ext}$, when $R_{int} = R_{ext}$).[45] When the average power was normalized by membrane area, the performance of single cell and double-stacked cell configurations were quite similar (Fig. 5, inset), indicating that boosting overall power production was possible by stacking multiple cells while maintaining the performance of the single cell.

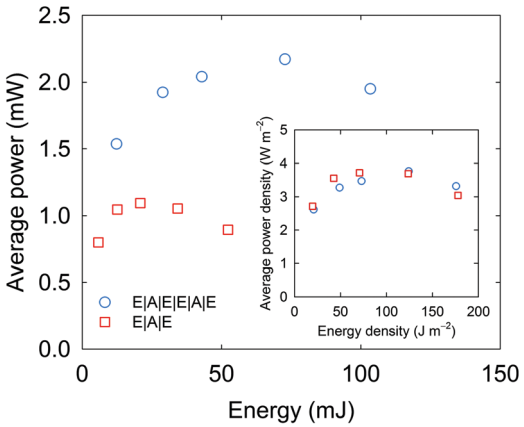

Fig. 5 Boosting the energy and power production by stacking cells. The energy harvesting performance was evaluated in the single cell (E|A|E, squares) and double-stacked cell (E|A|E|E|A|E, circles) by varying the load (R_{ext} = 2, 3, 4, 6, 10 Ω). E stands for electrode and the A stands for anion-exchange membrane (Fig. S4, ESI†). The membrane area (~3 cm^2 for each cell) was used to normalize the performance (inset).

The overall cell voltage and power production could also be increased by using an alternative array of cation- and anion-exchange membranes, in a "membrane-stacked cell" that is analogous to a RED cell (Fig. S4, ESI†). However, the average power density of the membrane-stacked cell normalized to membrane area was lower than that achieved for the single cell. The decrease in membrane-area normalized power density was due to the lower open-circuit cell voltage per number of ion-exchange membranes used in the cell as well as an increase in the membrane resistance. As a result, the power density of the concentration flow cell could be further increased by adding more ion-exchange membranes, but the gain would not be beneficial if the cost of ion-exchange membranes and reactor modification exceeded the value of the increased power. An additional challenge with increasing the number of ion-exchange membrane is that the achievable cell voltage would be limited by potential window of the CuHCF electrodes (Fig. S16, ESI†). Therefore, using a repeated array of CuHCF electrodes and anion-exchange membrane would be a better approach to increasing cell performance as opposed to using an array of ion-exchange membranes with only a single pair of electrodes.

Energy recovery efficiency of the concentration flow cell

To determine how efficiently the concentration flow cell converted salinity differences to the electricity, we calculated the theoretical net energy produced from a complete cycle (*i.e.*, the solutions were cycled through the cell until the synthetic seawater and freshwater stock solutions had the same salinity) and compared it to the theoretical amount of energy available from mixing the two solutions (Supplementary Note 1, ESI†). When operating the cell, there were primarily two processes that led to mixing between the HC and LC solutions: "controlled mixing" and "uncontrolled mixing". Controlled mixing is an inevitable consequence of converting a salinity difference into electricity, which arises as a result of Na^+-ion release/uptake by the CuHCF electrodes and Cl^--ion transport through the anion-exchange membrane. Assuming that only controlled mixing occurred was the baseline used to calculate an energy efficiency of 100%. Uncontrolled mixing in this cell could arise due to (1) imperfect perm-selectivity of the anion-exchange membrane and electrode reactions over the course of a cycle and (2) solution trapped within the electrode pores remaining when the solution flow paths were switched between cycles.[44]

Accounting for imperfect perm-selectivity and electrode reactions yielded an energy efficiency of 73.8%, which was the ratio of the amount of energy that was actually recovered to the theoretical energy available from controlled mixing (Fig. 6a and Supplementary Note 1, ESI†). The magnitude of the loss from solution trapped in electrode pores when switching solutions between cycles depended on the ratio of the electrode pore volume to the flow channel volume, defined here as "*r*". As expected, the calculated energy efficiency decreased (Fig. 6a) and the concentration of HC and LC solutions rapidly changed (Fig. 6b) as more solution was present within the electrode pores (r = 0.2, 0.5, 1.0). To estimate r, we measured the electrode pore volume two ways, which yielded pore volume of 0.07 cm^3 g^{-1}

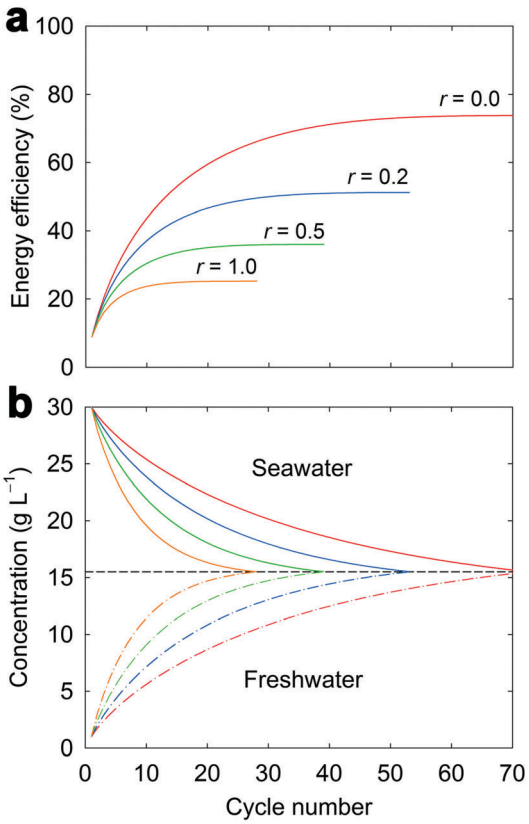

Fig. 6 Analysis of the energy efficiency. (a) Energy efficiency and (b) concentrations of seawater and freshwater calculated over cycles depending on the volume ratio (r) of the channel to the void of the electrode. An ideal system can extract energy from the salinity difference by redox reactions only (r = 0.0), while the energy efficiency would decrease (r = 0.2, 0.5, 1.0) due to the mixing between high and low concentration solutions absorbed in each electrode between cycles (Supplementary Note 1, ESI†).

(r = 0.09 for pores <300 nm, N_2 adsorption isotherms) and 1.86 $cm^3\ g^{-1}$ (r = 2.53 for pores <300 μm, mercury intrusion) (Supplementary Note 1, ESI†). Using these values, the energy efficiency of 60.8% was achieved when assuming that small pores affected the uncontrolled mixing and 15.3% when larger pores were considered for the calculation. Of course, these calculations only provide an estimate, as they do not provide insights into what fraction of the pore volume remained filled with the old solution when the solution paths are switched. In addition, a higher energy efficiency could be achieved by increasing R_{ext} (*i.e.*, decreasing the discharge current) due to the intrinsic tradeoff between the energy efficiency and power density. The efficiency of this system could also likely be improved by optimizing the discharging rate, electrode pore volume, and reactor configuration.

Conclusions

The concentration flow cell demonstrated here suggests that electrode and Donnan potentials can be combined to substantially increase power production. When using the salinity difference between synthetic seawater and river water, the peak power density for the concentration flow cell was 12.6 ± 0.5 W m^{-2} (average over a complete cycle = 3.8 ± 0.1 W m^{-2}), which was larger than the highest values reported to date for PRO (calculated: 9.2 W m^{-2}-membrane area, measured: 7.5 W m^{-2}),[11,12] RED (2.9 W m^{-2}),[26] and CapMix (0.4 W m^{-2}).[28] Although the peak power production achieved in the concentration flow cell was transient due to the finite charging capacity of battery electrodes and the dependency of the voltage on the charged state of the electrodes, the use of flow electrodes could allow for the constant power production while maintaining the high power density.[34,46] The power density was further increased using brine (300 g L^{-1}) in combination with river water (peak = 26.3 ± 1.3 W m^{-2}, average = 9.4 ± 0.9 W m^{-2}), which was noteworthy due to previously reported challenges in harvesting the higher potential energy contained in brines relative to seawater.[16] Although a previous PRO study reported a power density of 60 W m^{-2} using a brine (3 M NaCl),[12] current semi-permeable membranes cannot withstand the high pressures necessary to maintain this condition.[6,16] In RED, using brine (5 M NaCl) and river water (0.01 M NaCl) yielded a power density of 3.8 W m^{-2}, which was further increased to 6.7 W m^{-2} when the temperature was elevated (60 °C).[9] The lower power densities in RED relative to PRO for brines was due to in part decreased perm-selectivity of ion-exchange membranes with higher salinity differences, causing voltage loss.[5,9] In CapMix systems, to the best of our knowledge, no work has reported on generating electrical power using brines. A previous study showed that an electrochemical cell comprising of battery electrodes was able to develop cell voltages using highly concentrated solutions,[19] similar to what we reported in this study, indicating that the use of battery electrodes could overcome limitations of using brines in previous SGE technologies. A more detailed comparison of the power densities achieved in this study and past works using electrochemical systems is provided ESI† (Tables S1 and S2).

The cell voltage gained from the CuHCF electrodes and a single anion-exchange membrane allowed for a voltage gain that was equivalent to what can be achieved using two pairs of ion-exchange membranes in RED.[25] This result is significant in the context of the cost for salinity gradient technologies, as ion-exchange membranes are the most expensive component of these systems. Generating equivalent cell voltages with one membrane instead of four could significantly reduce the overall costs for real-world applications. When using real seawater or brines, several constraints may arise because various chemical species could cause detrimental effects on the system such as fouling[47] and unwanted ion transport across the membrane.[27,48] While little work has used real seawater or brines in RED and CapMix systems,[30,49] the general conclusion is that power production with real waters is lower than what is achievable using synthetic NaCl solutions. Recent work estimated that RED electricity production would be competitive against conventional renewable technologies if it could achieve a power density of 2.7 W m^{-2} per membrane area.[29] The average power density achieved here (3.8 ± 0.1 W m^{-2}) suggests that this

concentration flow cell may be a means to harvest salinity gradient energy in a cost effective manner, although a thorough cost analysis would be necessary to reach a definitive conclusion. Collectively, these findings suggest that simultaneously using electrode potentials and Donnan potentials in a single concentration flow cell is an attractive means to explore in the pursuit of sustainable and economically viable power generation from salinity gradients.

Acknowledgements

This research was supported by the National Science Foundation through awards CBET-1464891 and CBET-1603635 and internal seed grant funding from the Penn State Institutes for Energy and the Environment (PSIEE) and the Materials Research Institute (MRI).

References

1 O. Alvarez-Silva, C. Winter and A. F. Osorio, *Environ. Sci. Technol. Lett.*, 2014, **1**, 410–415.
2 R. S. Norman, *Science*, 1974, **186**, 350–352.
3 G. Z. Ramon, B. J. Feinberg and E. M. Hoek, *Energy Environ. Sci.*, 2011, **4**, 4423–4434.
4 International Energy Outlook 2016, http://www.eia.gov/forecasts/ieo/, accessed December 12, 2016.
5 N. Y. Yip and M. Elimelech, *Environ. Sci. Technol.*, 2014, **48**, 11002–11012.
6 A. P. Straub, A. Deshmukh and M. Elimelech, *Energy Environ. Sci.*, 2016, **9**, 31–48.
7 A. P. Straub, C. O. Osuji, T. Y. Cath and M. Elimelech, *Environ. Sci. Technol.*, 2015, **49**, 12551–12559.
8 G. Han, P. Wang and T.-S. Chung, *Environ. Sci. Technol.*, 2013, **47**, 8070–8077.
9 A. Daniilidis, D. A. Vermaas, R. Herber and K. Nijmeijer, *Renewable Energy*, 2014, **64**, 123–131.
10 B. E. Logan and M. Elimelech, *Nature*, 2012, **488**, 313–319.
11 N. Y. Yip, A. Tiraferri, W. A. Phillip, J. D. Schiffman, L. A. Hoover, Y. C. Kim and M. Elimelech, *Environ. Sci. Technol.*, 2011, **45**, 4360–4369.
12 A. P. Straub, N. Y. Yip and M. Elimelech, *Environ. Sci. Technol. Lett.*, 2013, **1**, 55–59.
13 E. Bar-Zeev, F. Perreault, A. P. Straub and M. Elimelech, *Environ. Sci. Technol.*, 2015, **49**, 13050–13058.
14 D. I. Kim, J. Kim, H. K. Shon and S. Hong, *J. Membr. Sci.*, 2015, **483**, 34–41.
15 N. Y. Yip and M. Elimelech, *Environ. Sci. Technol.*, 2013, **47**, 12607–12616.
16 N. Y. Yip, D. Brogioli, H. V. Hamelers and K. Nijmeijer, *Environ. Sci. Technol.*, 2016, **50**, 12072–12094.
17 D. Brogioli, *Phys. Rev. Lett.*, 2009, **103**, 058501.
18 B. Sales, M. Saakes, J. Post, C. Buisman, P. Biesheuvel and H. Hamelers, *Environ. Sci. Technol.*, 2010, **44**, 5661–5665.
19 F. La Mantia, M. Pasta, H. D. Deshazer, B. E. Logan and Y. Cui, *Nano Lett.*, 2011, **11**, 1810–1813.
20 D. Brogioli, R. Ziano, R. Rica, D. Salerno, O. Kozynchenko, H. Hamelers and F. Mantegazza, *Energy Environ. Sci.*, 2012, **5**, 9870–9880.
21 F. Liu, O. Schaetzle, B. B. Sales, M. Saakes, C. J. Buisman and H. V. Hamelers, *Energy Environ. Sci.*, 2012, **5**, 8642–8650.
22 M. C. Hatzell, R. D. Cusick and B. E. Logan, *Energy Environ. Sci.*, 2014, **7**, 1159–1165.
23 M. Ye, M. Pasta, X. Xie, Y. Cui and C. S. Criddle, *Energy Environ. Sci.*, 2014, **7**, 2295–2300.
24 D. A. Vermaas, M. Saakes and K. Nijmeijer, *Environ. Sci. Technol.*, 2011, **45**, 7089–7095.
25 J. W. Post, H. V. Hamelers and C. J. Buisman, *Environ. Sci. Technol.*, 2008, **42**, 5785–5790.
26 J. Moreno, E. Slouwerhof, D. Vermaas, M. Saakes and K. Nijmeijer, *Environ. Sci. Technol.*, 2016, **50**, 11386–11393.
27 D. A. Vermaas, J. Veerman, M. Saakes and K. Nijmeijer, *Energy Environ. Sci.*, 2014, **7**, 1434–1445.
28 T. Kim, M. Rahimi, B. E. Logan and C. A. Gorski, *Environ. Sci. Technol.*, 2016, **50**, 9791–9797.
29 A. Daniilidis, R. Herber and D. A. Vermaas, *Appl. Energy*, 2014, **119**, 257–265.
30 M. Tedesco, C. Scalici, D. Vaccari, A. Cipollina, A. Tamburini and G. Micale, *J. Membr. Sci.*, 2016, **500**, 33–45.
31 J. Veerman, M. Saakes, S. J. Metz and G. J. Harmsen, *Environ. Sci. Technol.*, 2010, **44**, 9207–9212.
32 D. A. Vermaas, S. Bajracharya, B. B. Sales, M. Saakes, B. Hamelers and K. Nijmeijer, *Energy Environ. Sci.*, 2013, **6**, 643–651.
33 M. Fernández, R. Wagterveld, S. Ahualli, F. Liu, A. Delgado and H. Hamelers, *J. Power Sources*, 2016, **302**, 387–393.
34 S. Porada, D. Weingarth, H. V. Hamelers, M. Bryjak, V. Presser and P. Biesheuvel, *J. Mater. Chem. A*, 2014, **2**, 9313–9321.
35 C. D. Wessells, S. V. Peddada, M. T. McDowell, R. A. Huggins and Y. Cui, *J. Electrochem. Soc.*, 2011, **159**, A98–A103.
36 D. A. Dzombak, R. S. Ghosh and G. M. Wong-Chong, *Cyanide in water and soil: chemistry, risk, and management*, CRC Press, 2005.
37 Y. Yang, C. Brownell, N. Sadrieh, J. May, A. Del Grosso, D. Place, E. Leutzinger, E. Duffy, R. He and F. Houn, *Clin. Toxicol.*, 2007, **45**, 776–781.
38 C. D. Wessells, R. A. Huggins and Y. Cui, *Nat. Commun.*, 2011, **2**, 550.
39 F. Scholz and A. Dostal, *Angew. Chem., Int. Ed. Engl.*, 1996, **34**, 2685–2687.
40 M. B. Soto and F. Scholz, *J. Electroanal. Chem.*, 2002, **521**, 183–189.
41 A. Widmann, H. Kahlert, H. Wulff and F. Scholz, *J. Solid State Electrochem.*, 2005, **9**, 380–389.
42 M. Pasta, R. Y. Wang, R. Ruffo, R. Qiao, H.-W. Lee, B. Shyam, M. Guo, Y. Wang, L. A. Wray and W. Yang, *J. Mater. Chem. A*, 2016, **4**, 4211–4223.
43 M. Pasta, C. D. Wessells, N. Liu, J. Nelson, M. T. McDowell, R. A. Huggins, M. F. Toney and Y. Cui, *Nat. Commun.*, 2014, **5**, 3007.

44 M. Marino, O. Kozynchenko, S. Tennison and D. Brogioli, *J. Phys.: Condens. Matter*, 2016, **28**, 114004.
45 S. Cheng, H. Liu and B. E. Logan, *Environ. Sci. Technol.*, 2006, **40**, 2426–2432.
46 V. Presser, C. R. Dennison, J. Campos, K. W. Knehr, E. C. Kumbur and Y. Gogotsi, *Adv. Energy Mater.*, 2012, **2**, 895–902.
47 D. A. Vermaas, D. Kunteng, M. Saakes and K. Nijmeijer, *Water Res.*, 2013, **47**, 1289–1298.
48 A. H. Avci, P. Sarkar, R. A. Tufa, D. Messana, P. Argurio, E. Fontananova, G. Di Profio and E. Curcio, *J. Membr. Sci.*, 2016, **520**, 499–506.
49 J. Lee, H. Yoon, J. Lee, T. Kim and J. Yoon, *ChemSusChem*, 2017, DOI: 10.1002/cssc.201601656.